A&A 583, A49 (2015)
DOI: 10.1051/0004-6361/201526812

Astronomy & Astrophysics

The role of binaries in the enrichment of the early Galactic halo⋆

I. *r*-process-enhanced metal-poor stars

T. T. Hansen[1], J. Andersen[2,3], B. Nordström[2,3], T. C. Beers[4], J. Yoon[4], and L. A. Buchhave[5,6]

[1] Landessternwarte, ZAH, Heidelberg University, Königstuhl 12, 69117 Heidelberg, Germany
e-mail: thansen@lsw.uni-heidelberg.de
[2] Dark Cosmology Centre, The Niels Bohr Institute, Copenhagen University, Juliane Maries Vej 30, 2100 Copenhagen, Denmark
[3] Stellar Astrophysics Centre, Department of Physics and Astronomy, Aarhus University, Ny Munkegade 120, 8000 Aarhus C, Denmark
[4] Department of Physics and JINA Center for the Evolution of the Elements, University of Notre Dame, Notre Dame, IN 46556, USA
[5] Harvard-Smithsonian Center for Astrophysics, Cambridge, MA 02138, USA
[6] Centre for Star and Planet Formation, Natural History Museum of Denmark, University of Copenhagen, 1350 Copenhagen, Denmark

Received 23 June 2015 / Accepted 1 August 2015

ABSTRACT

Context. The detailed chemical composition of most metal-poor halo stars has been found to be highly uniform, but a minority of stars exhibit dramatic enhancements in their abundances of heavy neutron-capture elements and/or of carbon. The key question for Galactic chemical evolution models is whether these peculiarities reflect the composition of the natal clouds, or if they are due to later (post-birth) mass transfer of chemically processed material from a binary companion. If the former case applies, the observed excess of certain elements was implanted within selected clouds in the early ISM from a production site at interstellar distances.
Aims. Our aim is to determine the frequency and orbital properties of binaries among these chemically peculiar stars. This information provides the basis for deciding whether local mass transfer from a binary companion is necessary and sufficient to explain their unusual compositions. This paper discusses our study of a sample of 17 moderately (*r*-I) and highly (*r*-II) *r*-process-element enhanced VMP and EMP stars.
Methods. High-resolution, low signal-to-noise spectra of the stars were obtained at roughly monthly intervals over eight years with the FIES spectrograph at the Nordic Optical Telescope. From these spectra, radial velocities with an accuracy of ∼100 m s^{-1} were determined by cross-correlation against an optimized template.
Results. Fourteen of the programme stars exhibit no significant radial-velocity variation over this temporal window, while three are binaries with orbits of typical eccentricity for their periods, resulting in a normal binary frequency of ∼18 ± 6% for the sample.
Conclusions. Our results confirm our preliminary conclusion from 2011, based on partial data, that the chemical peculiarity of the *r*-I and *r*-II stars is not caused by any putative binary companions. Instead, it was imprinted on the natal molecular clouds of these stars by an external, distant source. Models of the ISM in early galaxies should account for such mechanisms.

Key words. stars: abundances – stars: chemically peculiar – binaries: spectroscopic – Galaxy: halo – ISM: structure

1. Introduction

The pioneering HK survey of Beers, Preston, & Shectman (Beers et al. 1985, 1992) demonstrated the existence of substantial numbers of stars with metallicities well below those of globular clusters, and opened a new observational window on the epoch of early star formation in the Galactic halo. Modern surveys of metal-poor stars has greatly expanded the numbers of such stars known at present (see Ivezic et al. 2012, for a recent review), and spectroscopy with 8-m class telescopes have demonstrated a surprisingly uniform abundance pattern in the majority of them (Cayrel et al. 2004; Bonifacio et al. 2009; Aoki et al. 2013; Yong et al. 2013; Roederer et al. 2014a).

Since very metal-poor (VMP; [Fe/H] < −2.0) and extremely metal-poor (EMP; [Fe/H] < −3.0) halo stars probe the earliest epochs of chemical evolution in the Galaxy, their elemental-abundance patterns reflect the products of the primary heavy-element synthesis and enrichment processes in the early Galaxy. However, significant samples of chemically peculiar stars have been identified, in particular among the VMP and EMP stars. Because anomalies affecting a single element or group of elements must be produced by a small number of nucleosynthesis events (including possible single events), the chemically peculiar stars provide the opportunity to characterize the progenitors and enrichment processes that produced the abundance patterns in the long-lived metal-poor stars seen today.

However, in the relatively more metal-rich Population I and II stars, some chemical anomalies are known to be due to evolution in a close binary system (e.g. Ba and CH stars), in which a higher-mass binary companion has evolved to the asymptotic giant-branch (AGB) stage. Through processes

⋆ Appendices are available in electronic form at http://www.aanda.org

Table 1. *r*-I and *r*-II stars monitored for radial-velocity variation.

Stellar ID	RA (J2000)	Dec (J2000)	V	$B-V$	[Fe/H]	[Eu/Fe]	Class
HD 20	00:05:15	−27:16:18	9.24	0.54	−1.58	+0.80	*r*-I
CS 29497−004	00:28:07	−26:03:03	14.03	0.70	−2.81	+1.62	*r*-II
CS 31082−001	01:29:31	−16:00:48	11.67	0.77	−2.78	+1.66	*r*-II
HE 0432−0923	04:34:26	−09:16:50	15.17	0.73	−3.19	+1.25	*r*-II
HE 0442−1234	04:44:52	−12:28:46	12.91	1.08	−2.41	+0.52	*r*-I
HE 0524−2055	05:27:04	−20:52:42	14.01	0.88	−2.58	+0.49	*r*-I
HE 1044−2509	10:47:16	−25:25:17	14.35	0.67	−2.89	+0.94	*r*-I
HE 1105+0027	11:07:49	+00:11:38	15.65	0.39	−2.42	+1.81	*r*-II
HE 1127−1143	11:29:51	−12:00:13	15.89	0.68	−2.73	+1.08	*r*-II
HE 1219−0312	12:21:34	−03:28:40	15.94	0.64	−2.81	+1.41	*r*-II
HE 1430+0053	14:33:17	+00:40:49	13.69	0.59	−3.03	+0.72	*r*-I
HE 1523−0901	15:26:01	−09:11:38	11.13	1.06	−2.95	+1.82	*r*-II
CS 22892−052	22:17:01	−16:39:26	13.21	0.80	−2.95	+1.54	*r*-II
HE 2224+0143	22:27:23	+01:58:33	13.68	0.71	−2.58	+1.05	*r*-II
HE 2244−1503	22:47:26	−14:47:30	15.35	0.66	−2.88	+0.95	*r*-I
HD 221170	23:29:29	+30:25:57	7.71	1.02	−2.14	+0.85	*r*-I
CS 30315−029	23:34:27	−26:42:19	13.66	0.92	−3.33	+0.72	*r*-I

References. V and $B-V$ are from Beers et al. (2007), except for HD 221170, which is taken from Christlieb et al. (2004), and HE 1127−1143, which is from Henden et al. (2015). [Fe/H] and [Eu/Fe] are from Barklem et al. (2005), except for HE 1523−0901, where values from Frebel et al. (2007) are listed.

involving Roche-lobe overflow and/or wind accretion, the higher-mass star is expected to have contaminated the envelope of its surviving companion with any elements that formed during its final evolutionary stages. This mechanism could explain the presence of elements produced in the early Universe by stars more massive than ∼0.7 $M_{\odot}$ (i.e. with main-sequence lifetimes less than the Hubble time), but does of course require the presence of a binary companion, which by now is presumably a white dwarf or neutron star.

Hence, for the chemically peculiar VMP and EMP stars, a crucial first step is to establish whether any such putative binary companions actually exist, and to determine their main orbital parameters (i.e. period, semi-major axis, and eccentricity). This requires radial-velocity monitoring of adequate precision and duration for a sufficiently large sample of stars. High spectroscopic resolution ($R \gtrsim 30\,000$) allows one to determine radial velocities efficiently by cross-correlating even a relatively low signal-to-noise ratio (S/N) spectrum with an appropriate template, while long-term thermal and mechanical stability of the spectrograph employed is needed in order to detect variations with amplitudes below 1 km s^{-1}. As we demonstrate below, the FIES spectrograph at the 2.56-m Nordic Optical Telescope (NOT), which we have used to carry out our programme, meets these requirements.

This paper is the first in a series that explores the nature of three broad classes of chemically peculiar metal-poor halo stars. Here we consider the nature of VMP and EMP stars that exhibit moderate-to-large enhancements of elements associated with the rapid neutron-capture process, the so-called *r*-I and *r*-II stars, respectively. Other papers in this series consider samples of carbon-enhanced metal-poor (CEMP) stars (see Beers & Christlieb 2005): the CEMP-no stars (which exhibit no over-abundances of neutron-capture process elements; Paper II), and the CEMP-*s* stars (which exhibit over-abundances of elements originating in the slow neutron-capture process; Paper III).

This paper is structured as follows: Sect. 2 describes the sample of *r*-process-enhanced stars explored in our programme. Sections 3 and 4 describe in detail the observations, and the reduction and analysis procedures employed in the papers of this series. Section 5 summarizes our results, while Sect. 6 discusses these results and their implications for the progenitors of the *r*-I and *r*-II stars and the associated enrichment processes. Section 7 presents our final conclusions.

2. Sample stars

All but two of our sample stars were selected from the HK survey of Beers and colleagues (Beers et al. 1985, 1992) and the Hamburg/ESO survey of Christlieb and collaborators (Christlieb et al. 2008). The sample includes a number of the canonical examples of the *r*-process-element enhancement phenomenon; CS 22892−052, the first EMP star with detected Th (McWilliam et al. 1995; Sneden et al. 2000), CS 31082−001, the first EMP star with detected U (Hill et al. 2002; Cayrel et al. 2004), and HE 1523−0901, the most extremely *r*-process enhanced giant known (Frebel et al. 2007). All except HE 1523−0901 were analysed in the Hamburg/ESO R-process Enhanced Star (HERES) survey (Christlieb et al. 2004; Barklem et al. 2005). Accordingly, most of our programme stars are in the Southern Hemisphere (but north of declination $\delta \sim -25°$) and have $V \lesssim 16$, which is the practical limit for 1-h integrations with the NOT.

The sample stars are listed in Table 1, including their V magnitudes and $B-V$ colours, and reported [Fe/H] and [Eu/Fe] abundances. The last column of this table indicates whether a given star is considered to be a member of the moderately *r*-process-enhanced class (*r*-I; $+0.3 \leq$ [r/Fe] $\leq +1.0$) or the highly *r*-process-enhanced class (*r*-II; [r/Fe] $> +1.0$), according to the definitions of Beers & Christlieb (2005).

3. Observations

Spectra for our radial-velocity monitoring programme were obtained with the NOT, in service mode, using the FIES spectrograph[1], which has been used successfully for exo-planet

[1] http://www.not.iac.es/instruments/fies/

research (Buchhave et al. 2012). The spectra cover the wavelength range 3640 Å−7360 Å in 78 orders, at a resolving power of $R \sim 46\,000$. The S/N of the spectra is ∼10 on average, but ranges from ∼2 to ∼20. A S/N of ∼10 is obtained in ∼20 min for a star of $V = 14.5$, so a typical clear night yielded ∼10–15 spectra of the stars in Table 1. Integrations of 900 s or longer were split into three exposures, in order to enable effective cosmic ray rejection.

The observing strategy was based on the assumed analogy with the Ba II and CH binaries found by McClure (1984) and McClure et al. (1980) to have periods of the order of ∼300−3000 days and amplitudes of ∼3−10 km s^{-1}. Accordingly, spectra have been obtained at roughly monthly intervals since June 2007, and reduced immediately, so that follow-up of any variable objects could be planned efficiently. As we demonstrate, this strategy has worked well.

4. Reduction and analysis

The observations were reduced with pipeline software originally developed by Lars Buchhave to deliver high-precision radial velocities of exo-planet host stars from echelle spectrographs, in particular the FIES instrument (Buchhave 2010).

This reduction procedure includes all the normal steps, such as bias subtraction, division by a flat-field exposure, cosmic ray removal, and 2D order extraction. Sky background is only significant for the faintest stars if observed close to the full Moon, which was avoided in the nightly planning. Moreover, even substantial amounts of scattered moonlight are harmless if the two cross-correlation peaks are well separated, which is virtually always the case for our high-velocity programme stars.

For the wavelength calibration, a separate wavelength solution is created for each target spectrum, using Th-Ar calibration spectra taken just before each science frame. This procedure has been found to yield adequate velocity stability, as we demonstrate below.

4.1. Multi-order cross-correlation

With the reduced spectra in hand, multi-order cross-correlation against an optimized template spectrum is then performed, using software also developed by L. Buchhave (Buchhave 2010). The radial velocity from each individual order is determined by a Gaussian fit to the peak of the cross-correlation function (CCF); their mean value, weighted by the total photon count in each order, is taken as the final radial velocity from the observation.

Performing the cross-correlation order-by-order enables us to hand-pick the spectral regions to be used in the correlation, including regions with strong absorption lines and excluding regions with only a few and/or weak lines, which is a significant advantage when dealing with spectra of stars of such peculiar chemical compositions. Filtering is also applied to the spectrum before the cross-correlation to remove unwanted frequencies. The filters are carefully optimized for each star to remove noise while retaining even the narrowest stellar absorption lines.

4.2. Optimization of the template spectra

The choice of the template spectrum for the cross-correlation is crucial for the accuracy of the resulting radial velocities, especially in these spectra where the usual iron-peak elements only show weak lines, but strong lines exist from the normally rare neutron-capture elements.

Four different recipes have been used to construct the template spectra, depending on the quality of the target spectra: "Strongest", "Co-add", CS 31082−001, and "Delta". The Strongest template is the spectrum of a given star with the maximum signal level for that star. The advantage of using a spectrum of the same star as a template is the perfect match to the observed spectrum; the disadvantage is that a template with relatively low S/N will introduce noise into the correlation. The Co-add template is constructed by shifting a selection of the best spectra of the star to a common radial velocity and co-adding them. This results in a template with high S/N (which is also a perfect match for the target spectra), and will generally allow more orders to be included in the correlation, compared to a correlation with the strongest single spectrum as template. However, when creating the Co-add template, an initial correlation with the strongest spectrum as template is used to determine the shift of the other spectra. Any small residual shift will then broaden the spectral lines in the Co-add template spectrum and yield less precise results in the final correlation.

For the fainter stars, the Strongest template may introduce too much noise into the correlation, and a good Co-add template cannot then be constructed. Instead, a Co-add template from a bright star with a very similar spectrum may then be used as template; for these stars we have used CS 31082−001 in this manner. The final template option, used here for the faintest stars, is the Delta template, a synthetic spectrum consisting of δ functions at the (solar) wavelengths of selected lines. Sample spectra of the faint stars have been inspected for strong lines to be included in the Delta template spectrum. Correlation with this template yields velocities on an absolute scale, and has thus also been used to determine the absolute velocity of the other templates and to convert all velocities to an absolute scale.

4.3. Standard stars

A few well-established radial-velocity standard stars from Table 2 of Udry et al. (1999) were observed on every usable observing night in order to monitor any zero-point variations in the velocities. These are listed in Table 2, along with our mean (heliocentric) velocities and dispersions for these stars. The mean difference of our velocities from the standard values is 73 m s^{-1}, with a standard deviation of 69 m s^{-1}. This demonstrates that our results for the target stars are on a system consistent with that of Udry et al. (1999), and that the accuracy of our results is not limited by the stability of the spectrograph.

4.4. Error estimates

The internal error on the mean velocity from each spectrum is calculated as the standard deviation of the velocities from the individual orders used in the correlation. It is listed along with each observed velocity in Appendix A, and is used to plot the error bars of the data in the orbital plots shown in Fig. 2. For each star, the average internal error on the velocities is computed as the mean of these internal standard deviations, and is used to assess the quality of the correlation and the order selection.

The *external* standard deviation, σ, of the radial-velocity observations for each star, given in Table 2 for the radial-velocity standards and in Table 3 for the programme stars, is computed as

$$\sigma = \sqrt{\frac{1}{N-1}\sum_{j-0}^{N-1}(v_j - \bar{v})^2}. \quad (1)$$

Table 2. Results for the observed radial-velocity standard stars.

Stellar ID	RA (J2000)	Dec (J2000)	B	V	RV mean (km s^{-1})	σ (km s^{-1})	Nobs	ΔT (days)
HD 3765	00:40:49	+40:11:14	8.30	7.36	−63.35	0.033	60	2672
HD 38230	05:46:02	+37:17:05	8.19	7.36	−29.14	0.035	46	2771
HD 79210	09:14:23	+52:41:12	9.07	7.63	+10.45	0.048	29	2746
HD 115404	13:16:51	+17:01:02	7.46	6.52	+7.67	0.036	34	2891
HD 151541	16:42:39	+68:11:18	8.32	7.56	+9.44	0.028	30	2857
HD 182488	19:23:34	+33:13:19	7.15	6.36	−21.65	0.035	61	2072
HD 197076	20:40:45	+19:56:08	7.06	6.44	−35.37	0.052	26	2857

Table 3. Mean heliocentric radial velocities, standard deviations, and time-span covered for the programme stars.

Stellar ID	Nobs	Template	RV mean (km s^{-1})	σ (km s^{-1})	ΔT (days)	Binary
HD 20	14	Strongest	−57.914	0.041	2603	No
CS 29497−004	12	Co-add	+105.008	0.366	2583	No
CS 31082−001	24	Co-add	+139.068	0.105	2642	No
HE 0432−0923	18	Delta	−64.800	0.988	2737	No
HE 0442−1234	28	Co-add	+237.805	8.294	2618	Yes
HE 0524−2055	13	CS 31082−001	+255.425	0.195	2338	No
HE 1044−2509	14	Delta	+365.789	17.110	1887	Yes
HE 1105+0027	9	Delta	+76.197	0.496	1573	No
HE 1127−1143	7	Delta	+229.157	0.454	1998	No
HE 1219−0312	5	Delta	+162.416	1.094	2171	No
HE 1430+0053	20	Co-add	−107.749	0.426	2493	No
HE 1523−0901	34	Co-add	−163.271	0.284	2594	Yes
CS 22892−052	19	Co-add	+13.549	0.164	2174	No
HE 2224+0143	24	Co-add	−113.085	0.190	2420	No
HE 2244−1503	14	Delta	+147.928	0.246	2207	No
HD 221170	30	Strongest	−121.201	0.105	2174	No
CS 30315−029	14	Co-add	−169.346	0.352	2672	No

Imperfect guiding and centring of the star on the fibre end along with imperfect cancellation of changes in ambient temperature and atmospheric pressure, etc., contributes to small variations in the derived radial velocities, which are reflected in the standard deviations of the constant programme and radial-velocity standard stars.

For the three detected binaries in our sample, the above value for σ is inflated due to the orbital motion, and the relevant uncertainty estimate is the σ from the orbital solutions given in Table 4.

5. Results

The results of our radial-velocity monitoring of the sample stars are summarized in Table 3, which lists the star name, the number of observations (Nobs), the template used for each star, the mean (heliocentric) radial velocity and standard deviation over the observed time span (ΔT), and the binary status for each star. The individual observed heliocentric radial velocities are listed in Appendix A, together with the Julian dates of the observations and their internal errors.

As can be seen from a glance at Table 3, fourteen of our stars exhibit no variation in their radial velocities at the level of a few hundred metres per second over the eight years of monitoring. For the brighter targets, the standard deviations of the observed velocities are ∼100 m s^{-1} (dominated by centring and guiding errors), rising to ∼1 km s^{-1} for the fainter targets, due to the lower S/N of their spectra. Moreover, least-squares fits of the velocities vs. time reveal no net trends over the observing period.

5.1. Comparison with literature data

Table B.1 lists mean radial velocities (based on high-resolution spectroscopy) from the literature for the single stars in our sample, along with the complete time span covered by the combined data (including our own measurements). Most of the stars have only been observed once earlier by Barklem et al. (2005), for which they estimate an error of a few km s^{-1}, and we find excellent agreement between their results and ours. For HD 20 and HD 221170, radial velocities were also reported by Carney et al. (2003), who list 13 observations for HD 20 and 18 for HD 221170, spanning 4641 and 5145 days, with (external) standard deviations of 0.41 and 0.61 km s^{-1}, respectively. Their mean radial velocities of −57.18 km s^{-1} and −121.77 km s^{-1} are consistent with our results, given the slight offset of the CfA velocities from the system of Udry et al. (1999).

For the faint star HE 1219−0312, our five measurements with the 2.5-m NOT span 2171 days from 2007, while the five epochs of the earlier Hayek et al. (2009) VLT/UVES observations span ∼400 days. The standard deviations (∼1 km s^{-1}) and their mean radial velocity (163.1 km s^{-1}) are similar to ours, and consistent with our own conclusion that this star is single.

From inspection of Table B.1 it is clear that, while the coverage of the listed spans for most of the single stars is rather sparse, the spans themselves are from two to five times longer than those obtained during the course of our own radial-velocity monitoring programme. The lack of observed variations beyond what can be accounted for by the expected errors across multiple spectrograph/telescope combinations strengthens our claim that the stars we classify as single are indeed so.

Table 4. Orbital parameters of the binary systems in the sample.

Parameter	HE 0442−1234	HE 1044−2509	HE 1523−0901
Period (days)	2515.2 ± 5.5	36.561 ± 0.009	303.05 ± 0.25
T_0 (BJD)	2 457 918.3 ± 1.0	2 455 737.1 ± 0.1	2 455 068.0 ± 4.1
K (km s^{-1})	12.541 ± 0.016	27.024 ± 0.96	0.350 ± 0.003
γ (km s^{-1})	236.35 ± 0.01	360.22 ± 0.57	−163.23 ± 0.003
e	0.767 ± 0.001	0.000[a]	0.163 ± 0.010
ω °	316.6 ± 0.1	90.00	81.7 ± 4.7
$a \sin i$ ($R_\odot$)	400.2 ± 1.2	19.6 ± 0.7	2.07 ± 0.02
$f(m)$ ($M_\odot$)	0.136 ± 0.001	0.075 ± 0.009	1.3E-5 ± 4E-8
σ (km s^{-1})	0.28	1.88	0.11
$R_{\rm Roche}$ ($R_\odot$, M_1 = 0.8 $M_\odot$, M_2 = 0.6 $M_\odot$)	59	13	53
$R_{\rm Roche}$ ($R_\odot$, M_1 = 0.8 $M_\odot$, M_2 = 1.4 $M_\odot$)	770	46	220

Notes. [(a)] Eccentricity for HE 1044-2509 fixed to zero.

5.2. Binary orbits

Three of our stars are spectroscopic binaries, as first reported by Hansen et al. (2011). HE 0442−1234 was found already by P. Bonifacio et al. (priv. comm.) to be a long-period binary, while HE 1044−2509 and HE 1523−0901 are new discoveries from our programme. All three orbits have now been fully completed, with particular attention being paid to assessing the reality of the very low-amplitude velocity variations of HE 1523−0901. After rejecting early observations made under poor conditions (strong moonlight, poor seeing), and with now almost nine orbital revolutions completed, we have satisfied ourselves that this nearly face-on orbit is real and the orbital parameters are reliable (see below).

In contrast to this result, our own (far more accurate) velocity data clearly disprove the putative orbit suggested by Preston & Sneden (2001) for CS 22892-052, with $P \sim$ 128 days and $K \sim 1.0$ km s^{-1}. Both this star and CS 31082−001 are clearly single stars, as can be seen from Table 3 and Fig. 1, where the derived radial velocities for the two stars are plotted as a function of time. Our results for stars observed with similar time spans and accuracies in parallel parts of our overall programme show that binaries with orbital periods of 20−30 years are detected with certainty even after the first couple of years with ∼monthly observations.

The observed $K \sim 350$ m s^{-1} of HE 1523−0901 is the smallest measured with certainty in our programme, highlighting the null result for the other, single stars. The corresponding tiny mass function implies either a companion of mass in the brown-dwarf range (for $i \sim 90°$), or a very low orbital inclination, or a combination of both. Assuming $i \lesssim 2.5°$ leads to a secondary mass in the late M-dwarf range, 0.25 $M_\odot$ – still plausible within the statistics for a single case in a sample of several tens of potential (southern) r-I and r-II targets.

Long-period envelope pulsations are a potential alternative origin of radial-velocity variations for this and other cool giant stars, and we have also found some strongly carbon-enhanced VMP and EMP stars showing similar low-level radial-velocity fluctuations. The frequency of real spectroscopic binaries with very low inclinations is far too low to ascribe all such low-amplitude velocity variations to binary orbital motion, and most marginal variations are, in the end, found not to be strictly periodic. Thus, it may be that low-level pulsations, rather than velocity accuracy, may set the ultimate limit to the length of the binary periods that can be reliably detected by the radial-velocity technique, as is the case for exo-planet orbits.

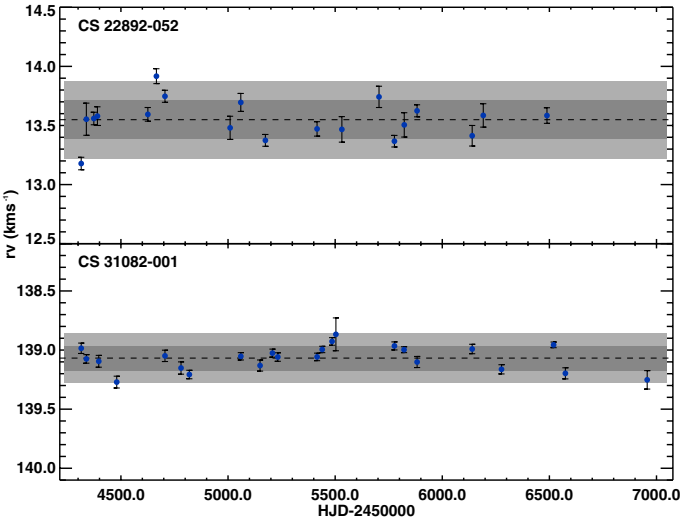

Fig. 1. Heliocentric radial velocities derived for CS 22892−052 (*top*) and CS 31082−001 (*bottom*), as a function of time. Dashed lines: mean radial velocity; grey shaded areas: 1σ and 2σ regions around the mean.

Our current knowledge of the pulsational characteristics of late-type evolved stars is derived from the systematic microlensing surveys of MACHOs towards the Magellanic Clouds (Wood 2000; Riebel et al. 2010). The late-type pulsators with periods of 200−1000 days are typically C-type AGB stars or Mira variables, but stars below the tip of the red-giant branch have shorter periods, and the cause of their light variation is not known. Precise light and colour curves for field VMP/EMP stars with equally well-determined distances, or at least log q, periods or pseudo-periods of the order of a year, and phasing consistent with pulsations would be needed to settle the issue definitively. However, obtaining them with sufficient accuracy is not an easy task, and none has been reported for HE 1523−0901.

The final orbital elements for the three binary systems among our programme stars are listed in Table 4, and velocity curves with all available observations are shown in Fig. 2.

6. Discussion

6.1. Binary frequency of r-I and r-II stars

The salient result of our study is that only 3 of our 17 programme stars are binaries, while 14 are confirmed to be single stars, a binary frequency of ∼18 ± 6%.

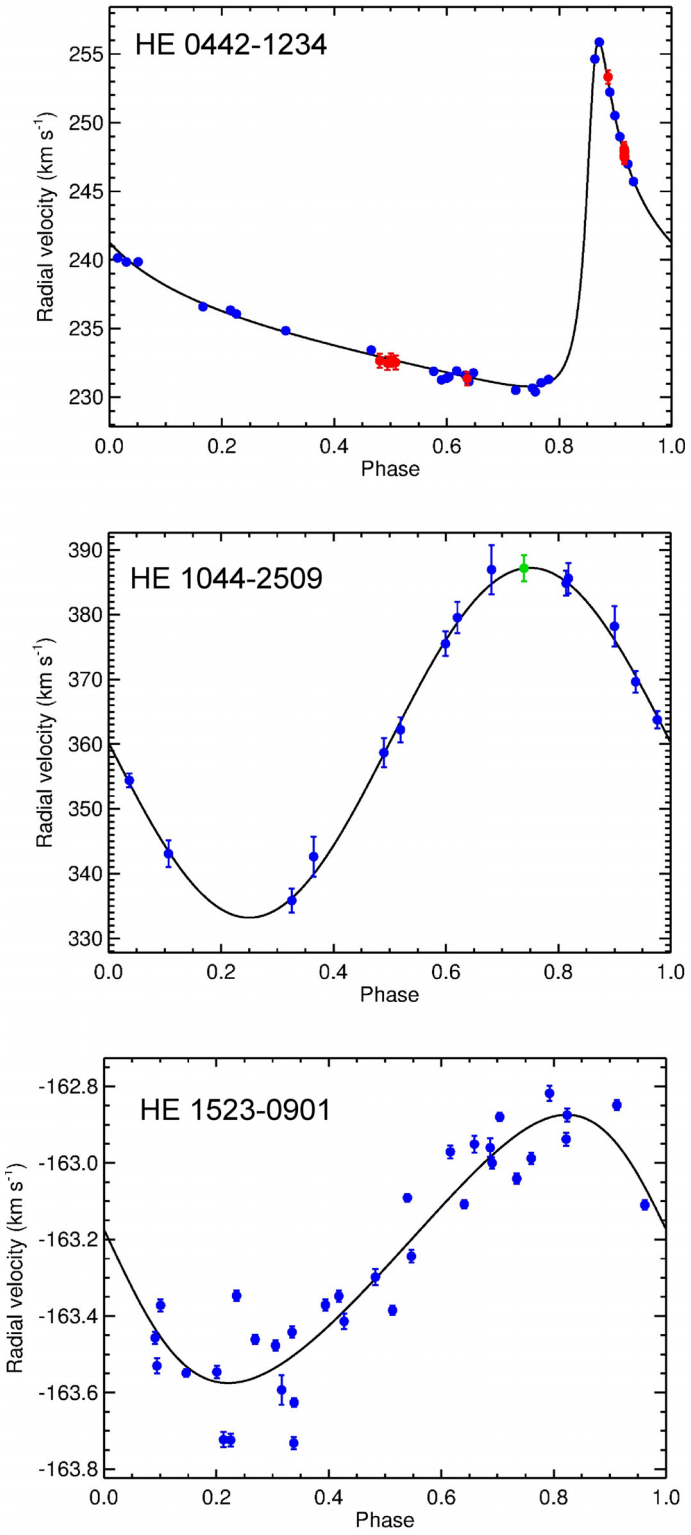

Fig. 2. Orbital solutions for the three binary systems found in our programme. *Top*: HE 0442−1234 (blue this work, red P. Bonifacio, priv. comm.), *middle*: HE 1044−2509 (blue this work, green Barklem et al. 2005) and *bottom*: HE 1523−0901.

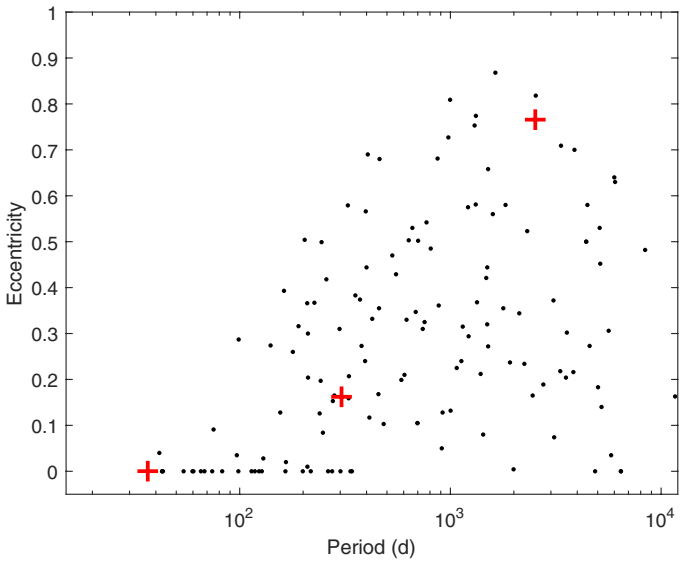

Fig. 3. Period – eccentricity diagram for giant binaries. Dots: 141 members of Galactic open clusters (Mermilliod et al. 2007; Mathieu et al. 1990); red plus signs: the three *r*-I and *r*-II binaries discussed in this paper.

Our sample is relatively small, since HERES stars south of the NOT limit could not be observed by us, but only two other *r*-process-enhanced stars, the *r*-II star HE 2327−5642 and the *r*-I star CS 22183−031, have been reported in the literature to show variable radial velocities. HE 2327−5642 was discovered by Mashonkina et al. (2010); their data cover a range of ∼4.3 years, during which the radial velocity of the star varied by ∼20 km s^{-1}. The other star, CS 22183−031, is included in the sample of Roederer et al. (2014b), who reported on the identification of nine new *r*-process-enhanced stars. The radial-velocity data for neither of these stars is sufficient to derive an orbital solution for the systems. The bright *r*-I star HD 115444 (Westin et al. 2000) was not observed in our programme, but literature data confirm (with variations of no more than 1 km s^{-1} over a sparsely-sampled range of 24 years; see Table B.2) that it too is vey likely a single star, as is its *r*-process-*poor* counterpart HD 122563 (with variations of no more than 1.5 km s^{-1} over a sparsely-sampled range of 59 years; see Table B.2).

In summary, the binary frequency of 18 ± 6% found here for the *r*-I and *r*-II stars is completely consistent with the 16 ± 4% of binaries with periods up to 6000 days found by Carney et al. (2003) in their survey of 91 metal-poor field giants, and the ∼22% binaries with periods up to ∼15 000 days found by Mermilliod et al. (2008) in their sample of ∼1300 Population I giants in Galactic open clusters. A binary frequency of 100% for this class of VMP and EMP stars is clearly ruled out, a conclusion that would only be reinforced if HE 1523−0901 were eventually proved to be a single pulsating star rather than a binary with a nearly face-on orbit.

Overall, we can thus conclude that the observed dramatic excess of *r*-process elements in our sample of stars is not just a surface effect produced locally by a binary companion, but rather was produced by a remote source and imprinted on the parent clouds across interstellar distances. It also seems hard to imagine how the local binary scenario could produce stars like HD 122653, with a *deficit* of *r*-process elements relative to the standard abundance pattern.

6.2. Frequency and properties of r-I and r-II binaries

The distribution of periods and eccentricities of our three binaries is also fully as expected for binary systems with normal giant primary stars. This is illustrated most simply in Fig. 3, which shows a period – eccentricity diagram constructed from

the orbital data for 141 giant binary members of (Population I) Galactic open clusters by Mermilliod et al. (2007) and Mathieu et al. (1990), plotted as dots, while our three binaries are shown as red plus symbols. As seen, their orbital eccentricities are completely normal for giant binaries, which are typically tidally circularized for periods up to ∼150 days, depending on age and stellar mass, and show no sign of tidal or other processes that could be connected to their outstanding chemical peculiarity. In contrast, the transition between circular and eccentric orbits seems to occur at periods of ∼4−800 days for binaries with former AGB companions.

Further information on the presently unseen companions can be derived by considering the volume available to them during their evolution; i.e. their Roche-lobe radii, which can be computed from the observed orbital separation (assuming no exchange or loss of mass and angular momentum) and a range of assumed stellar masses. We first adopt a common mass of 0.8 $M_{\odot}$ for the observed EMP giants and assume that the companion is a (sub)dwarf (i.e. unevolved) star of mass 0.6 $M_{\odot}$, at least three magnitudes fainter than the star we do see. The present radius of the latter can be estimated from the adopted mass and a typical log $g \sim 1.5$ dex, i.e. $R \sim 30\ R_{\odot}$.

With the observed orbital elements, notably $a_1 \sin i$ and the mass function, we then adjust i until the computed M_2 reaches 0.6 $M_{\odot}$, and calculate the corresponding Roche-lobe radii, which are given in Table 4. For HE 0442−1234, the minimum secondary mass is 0.67 $M_{\odot}$ already for $i = 90°$; for HE 1044−2509 and HE 1523−0901, we find $i = 62°$ and 1.3°, respectively, for a secondary mass of 0.6 $M_{\odot}$.

However, we might alternatively assume that the companions were initially *more* massive than 0.8 $M_{\odot}$, i.e. in the range of 1−8 $M_{\odot}$, where they would have gone through the AGB phase and likely have evolved into now-invisible white dwarfs (WDs) with typical masses of 0.6 $M_{\odot}$, and thus identical $R_{\rm Roche}$ to the ones found above. It is possible that the WD might also have the maximum WD mass of 1.4 $M_{\odot}$, in which case the entire system would be much larger and the Roche-lobe radius of the companion a larger share of that again. Nominal Roche-lobe radii for this case are also given in Table 4, and illustrate the dramatic change in the space available to the star during its evolution, depending on its assumed mass.

For HE 1044−2509, even this $R_{\rm Roche}$ is still too small to accommodate a typical AGB star of ∼200 $R_{\odot}$. In any case, the observed absence of any *s*-process signatures indicates that mass transfer from a putative AGB companion did not happen in any of these systems, while a supernova explosion of a putative, even more massive companion would likely have disrupted the binary system (Tauris & Takens 1998).

In summary, binary systems seem to occur as a normal part of the formation of *r*-process-enhanced metal-poor stars, and are unrelated to the process by which they acquired their outstanding chemical anomalies.

6.3. Origin of r-I and r-II stars

The separation of *r*-process-enhanced stars into the *r*-I and *r*-II classes was originally a matter of convenience, since the heavy-element abundance patterns of the most enhanced stars could be more easily observed due to their relatively stronger lines at low metallicity. As the sample of such stars has grown, it has become clear that these classes also exhibit rather different behaviour with metallicity; the *r*-II stars are found in a relatively narrow range of metallicity near [Fe/H] ∼ −3.0, while the *r*-I stars cover a larger range of metallicity, −3.5 < [Fe/H] < −1.5 (Beers 2013). It remains unclear whether this constraint implies that different classes of astrophysical progenitors might be responsible for the *r*-I and *r*-II stars, or whether the initial *r*-process content in the natal clouds of the *r*-I stars has simply been diluted by the elemental mix of standard chemical evolution.

All of our programme stars are giants. However, it is important to note that Aoki et al. (2010) have shown that the star SDSS J2357−0052 is a cool ($T_{\rm eff}$ ∼5000 K) main-sequence dwarf with [Fe/H] = −3.4, and [Eu/Fe] = +2.0, making it simultaneously the lowest metallicity and most Eu-enriched *r*-II star yet found. This star is of particular interest, as all previous *r*-process-enhanced stars identified to date have been in more evolved stages of evolution. Since dwarfs with the temperature of SDSS J2357−0052 do not have convective atmospheres, it can be reasonably concluded that the *r*-process-enhancement phenomenon is not due to some chemical peculiarity arising from the presence of a convective envelope in such stars. Unfortunately, although this star is sufficiently bright ($V \sim 15.6$) for the programme described above, it was discovered too late to be included in our target list, but the results of radial-velocity monitoring over about a year by Aoki et al. did not reveal any evidence of significant variation.

The nine newly recognized *r*-process-enhanced stars (based on high-resolution spectroscopic follow-up of HK survey stars) by Roederer et al. (2014b) include subgiants and the field equivalents of red horizontal-branch stars, reaffirming that *r*-process enhancement is not an evolutionary effect in the stars. Roederer et al. (2014b) also compare the abundance pattern of the light elements in their *r*-process-enhanced stars with that of *non-r*-process-enhanced stars with similar stellar parameters. No evidence was found to indicate that the *r*-process-enhanced stars have different abundance patterns for the light elements than for the comparison sample, leading the authors to conclude that the event(s) producing the high levels of *r*-process material seen in these stars do not produce a distinct light-element abundance pattern. Neither does the large *r*-process enhancement seem to be coupled to the carbon and nitrogen abundances in the stars, although a few of the *r*-II stars are found to also be enhanced in carbon, the most well-known example being CS 22892−052 (Sneden et al. 2000).

Mashonkina et al. (2010) explored the Sr, Ba and Eu abundances for a number of *r*-I and *r*-II stars. They found very similar [Ba/Eu] abundance ratios for the two groups ([Ba/Eu] ∼ +0.60), but the mean [Sr/Eu] ratio differed by 0.36 dex between the two groups, with the *r*-II stars having the lowest ratio, [Sr/Eu] = −0.93. The authors argued that elements from the first and second *r*-process peak are of common origin in the *r*-II stars, whereas for the *r*-I stars the picture is less clear.

Competing scenarios for the origin of the *r*-I and *r*-II stars invoke non-spherical, jet-producing supernova explosions or neutrino winds from merging neutron star binaries. Detailed observations of the abundance patterns predicted from the two competing scenarios may be the best guide to identifying the production site(s), but the frequency of these stars (∼3% among VMP and EMP stars; Roederer et al. 2014b) provides another clue; any jets in such scenarios must be highly collimated in order to selectively enrich only a small fraction of molecular clouds in the early ISM.

One circumstance is worthy of note, although its interpretation is currently unclear: Of the two *r*-II stars with secure detections of uranium, CS 31082−001 exhibits the so-called "actinide boost" (Hill et al. 2002), and has now been shown to be a single star, while the detailed *r*-process abundance pattern of the newly

identified binary HE 1523−0901 does not. While this may just be a result of small-number statistics on these very rare objects, it should be kept in mind as the sample grows; the details of their chemical-abundance patterns would appear to offer our most reliable clue to the origin of this difference.

7. Conclusions

In order to detect a possible link between the nature of the binary population among stars that exhibit moderate to strong enhancements in their *r*-process-element abundances and the origin of their peculiar abundance patterns, we have monitored the radial velocities of 17 such stars with high precision (∼100 m s^{-1}) over a period of eight years.

Of the 17 programme stars, 14 exhibit no radial-velocity variations during this period, and are thus presumably single, while three are binaries with normal orbital periods and eccentricities, yielding a normal binary frequency of ∼18% among these stars. Hence, there is no evidence that the *r*-process enhancement seen in the *r*-I and *r*-II stars is causally linked to the binary nature of the stars. Furthermore, the detection of *r*-process-element rich stars in dwarf, subgiant, giant, and horizontal-branch evolutionary phases shows that the enhancement phenomenon is also not linked to the evolution of the stars.

We conclude that the moderate-to-high *r*-process-element abundances derived for these stars must be an imprint of the clouds from which the stars were formed. Detailed abundance analysis of larger samples of *r*-I and *r*-II stars is required to better constrain the nature of the objects and the chain of events that polluted the natal clouds of these stars. Moreover, the mechanism(s) for such sporadic, inhomogeneous enrichment of the ISM in early galaxies, and their implication for understanding the observed chemical composition of high-redshift DLA systems, should be considered in the next generation of models for the formation and early chemical evolution of galaxies.

Acknowledgements. This paper is based on observations made with the Nordic Optical Telescope, operated by the Nordic Optical Telescope Scientific Association at the Observatorio del Roque de los Muchachos, La Palma, Spain, of the Instituto de Astrofisica de Canarias. We thank several NOT staff members and students for obtaining most of the observations for us in service mode. The work of T.H. was supported by Sonderforschungsbereich SFB 881 "The Milky Way System" (subproject A4) of the German Research Foundation (DFG). T.C.B. and J.Y. acknowledge partial support for this work from grants PHY 08-22648; Physics Frontier Center/Joint Institute or Nuclear Astrophysics (JINA), and PHY 14-30152; Physics Frontier Center/JINA Center for the Evolution of the Elements (JINA-CEE), awarded by the US National Science Foundation. J.A. and B.N. gratefully acknowledge financial support from the Danish Natural Science Research Council and the Carlsberg Foundation. B.N. gratefully acknowledges partial support from the National Science Foundation under Grant No. NSF PHY11-25915. Furthermore, we thank the referee for helpful comments.

References

Aoki, W., Honda, S., Beers, T. C., & Sneden, C. 2003, ApJ, 586, 506
Aoki, W., Beers, T. C., Honda, S., & Carollo, D. 2010, ApJ, 723, L201
Aoki, W., Beers, T. C., Lee, Y. S., et al. 2013, AJ, 145, 13
Barklem, P. S., Christlieb, N., Beers, T. C., et al. 2005, A&A, 439, 129
Bartkevicius, A., Sperauskas, J., Rastorguev, A. S., & Tokovinin, A. A. 1992, Balt. Astron., 1, 47
Beers, T. C. 2013, Nuclei in the Cosmos XII, Proc. Sci., PoS (NIC-XII), 56
Beers, T. C., & Christlieb, N. 2005, ARA&A, 43, 531
Beers, T. C., Preston, G. W., & Shectman, S. A. 1985, AJ, 90, 2089
Beers, T. C., Preston, G. W., & Shectman, S. A. 1992, AJ, 103, 1987
Beers, T. C., Flynn, C., Rossi, S., et al. 2007, ApJS, 168, 128
Bond, H. E. 1980, ApJS, 44, 517
Bonifacio, P., Spite, M., Cayrel, R., et al. 2009, A&A, 501, 519
Buchhave, L. A. 2010, Ph.D. Thesis, Univ. of Copenhagen
Buchhave, L., Latham, D. W., Johansen, A., et al. 2012, Nature, 486, 375
Carney, B. W., & Latham, D. W. 1986, AJ, 92, 60
Carney, B. W., Latham, D. W., Stefanik, R. P., et al. 2003, AJ, 125, 293
Carney, B. W., Gray, D. F., Yong, D., et al. 2008, AJ, 135, 892
Carrera, R., Pancino, E., Gallart, C., & del Pino, A. 2013, MNRAS, 434, 1681
Cayrel, R., Depagne, E., Spite, M., et al. 2004, A&A, 416, 1117
Christlieb, N., Beers, T. C., Barklem, P. S., et al. 2004, A&A, 428, 1027
Christlieb, N., Schörck, T., Frebel, A., et al. 2008, A&A, 484, 721
Famaey, B., Jorissen, A., Luri, X., et al. 2005, A&A, 430, 165
Frebel, A., Christlieb, N., Norris, J. E., et al. 2007, ApJ, 660, L117
Griffin, R., Gustafsson, B., Vieira, T., & Griffin, R. 1982, MNRAS, 198, 637
Hayek, W., Wiesendahl, U., Christlieb, N., et al. 2009, A&A, 504, 511
Hansen, T., Andersen, J., Nordström, B., Buchhave, L., & Beers, T. C. 2011, ApJ, 743, L1
Henden, A. A., Levine, S., Terrell, D., & Welch, D. L. 2015, Am. Astron. Soc. Meet. Abstr., 225, 336.16
Hill, V., Plez, B., Cayrel, R., et al. 2002, A&A, 387, 560
Hollek, J. K., Frebel, A., Roederer, I. U., et al. 2011, ApJ, 742, 54
Honda, S., Aoki, W., Ando, H., et al. 2004, ApJS, 152, 113
Ivezic, Z., Beers, T. C., & Juric, M. 2012, ARA&A, 50, 251
Kordopatis, G., Gilmore, G., Steinmetz, M., et al. 2013, AJ, 146, 134
Mashonkina, L., Christlieb, N., Barklem, P. S., et al. 2010, A&A, 516, A46
Mathieu, R. D., Latham, D. W., & Griffin, R. F. 1990, AJ, 100, 1899
McClure, R. D. 1984, ApJ, 280, L31
McClure, R. D., Fletcher, J. M., & Nemec, J. M. 1980, ApJ, 238, L35
McWilliam, A., Preston, G. W., Sneden, C., & Searle, L. 1995, AJ, 109, 2757
Mermilliod, J.-C., Andersen, J., Latham, D. W., & Mayor, M. 2007, A&A, 473, 829
Mermilliod, J.-C., Mayor, M., & Udry, S. 2008, A&A, 473, 829
Norris, J. E., Ryan, S. G., & Beers, T. C. 1996, ApJS, 107, 391
Preston, G. W., & Sneden, C. 2001, AJ, 122, 1545
Riebel, D., Meixner, M., Fraser, O., et al. 2010, ApJ, 723, 1195
Roederer, I., Lawler, J. E., Sneden, C., et al. 2008, ApJ, 675, 723
Roederer, I. U., Preston, G. W., Thompson, I. B., et al. 2014a, AJ, 147, 136
Roederer, I., Cowan, J. J., Preston, G. W., et al. 2014b, MNRAS, 445, 2970
Sneden, C., Cowan, J. J., Ivans, I. I., et al. 2000, ApJ, 533, L139
Soubiran, C., Bienaymé, O, Mishenina, T. V., & Kovtyukh, V. V. 2008, A&A, 480, 91
Tauris, T. M., & Takens, R. J. 1998, A&A, 330, 1047
Tsangarides, S. A., Ryan, S. G., & Beers, T. C. 2003, CNO in the Universe, eds. C. Charbonnel, D. Schaerer, & G. Meynet, ASP Conf. Ser., 304, 133
Udry, S., Mayor, M., & Queloz, D. 1999, PASPC, 185, 367
Wallerstein, G., Greenstein, J. L., Parker, R., Helfer, H. L., & Aller, L. H. 1963, ApJ, 137, 280
Westin, J., Sneden, C., Gustafsson, B., & Cowan, J. J. 2000, ApJ, 530, 783
Wilson, R. E. 1953, in General Catalogue of Stellar Radial Velocities (Carnegie Institution of Washington D.C. Publication), 601
Wilson, R. E., & Joy, A. 1950, ApJ, 111, 221
Wood, P. R. 2000, PASA, 17, 18
Woolley, R., & Harding, G. A. 1965, Royal Observatory Bulletin, 93, 363
Yong, D., Norris, J. E., Bessell, M. S., et al. 2013, ApJ, 762, 26

Pages 9 to 13 are available in the electronic edition of the journal at http://www.aanda.org

Appendix A: Individual heliocentric radial velocities measured for the programme stars

Table A.1. HD 20.

HJD	RV (km s^{-1})	$RV_{\rm err}$ (km s^{-1})
2 454 314.661653	−57.892	0.033
2 454 338.615723	−57.891	0.022
2 454 373.612652	−57.900	0.024
2 454 819.293270	−57.983	0.030
2 455 126.580295	−57.946	0.041
2 455 175.394755	−57.978	0.023
2 455 503.480513	−57.855	0.070
2 455 776.652777	−57.940	0.022
2 455 796.657395	−57.927	0.025
2 455 859.514789	−57.862	0.034
2 456 139.703103	−57.863	0.027
2 456 241.446457	−57.899	0.064
2 456 529.679820	−57.934	0.023
2 456 917.579578	−57.924	0.027

Table A.2. CS 29497−004.

HJD	RV (km s^{-1})	$RV_{\rm err}$ (km s^{-1})
2 454 373.642892	104.329	0.116
2 454 705.631179	104.873	0.065
2 454 780.500993	105.409	0.292
2 454 819.320354	105.561	0.084
2 455 175.419215	105.010	0.063
2 455 415.686599	104.941	0.061
2 455 439.606743	105.124	0.060
2 455 796.671082	105.434	0.077
2 455 858.545060	105.060	0.060
2 456 191.589163	105.050	0.045
2 456 530.687786	104.829	0.054
2 456 956.535485	104.471	0.094

Table A.3. CS 31082−001.

HJD	RV (km s^{-1})	$RV_{\rm err}$ (km s^{-1})
2 454 314.681742	138.985	0.044
2 454 338.656269	139.075	0.036
2 454 396.548819	139.095	0.050
2 454 480.372487	139.271	0.050
2 454 705.645953	139.049	0.048
2 454 780.529216	139.152	0.052
2 454 819.336946	139.207	0.036
2 455 059.684154	139.053	0.031
2 455 149.486943	139.131	0.047
2 455 207.337039	139.026	0.034
2 455 232.321077	139.059	0.036
2 455 415.734837	139.058	0.032
2 455 439.622078	138.995	0.027
2 455 485.577689	138.927	0.032
2 455 503.470979	138.867	0.139
2 455 776.741087	138.965	0.034
2 455 821.588602	138.997	0.025
2 455 882.542281	139.101	0.047
2 456 139.725335	138.991	0.040
2 456 276.485443	139.163	0.039
2 456 519.736731	138.956	0.024
2 456 574.672228	139.197	0.047
2 456 956.570319	139.252	0.078

Table A.4. HE 0432−0923.

HJD	RV (km s^{-1})	$RV_{\rm err}$ (km s^{-1})
2 454 338.702068	−64.948	0.983
2 454 373.722874	−64.876	1.097
2 454 396.715153	−66.294	1.602
2 454 406.637662	−64.942	1.710
2 454 459.590478	−62.264	2.232
2 454 480.431485	−65.026	1.202
2 454 516.372208	−64.832	0.592
2 454 780.591463	−64.462	1.896
2 454 819.450079	−64.460	1.351
2 455 075.713863	−65.352	1.544
2 455 176.552628	−64.543	0.684
2 455 232.419859	−65.290	1.106
2 455 531.609740	−64.654	1.303
2 455 620.393797	−63.236	2.281
2 455 944.449119	−66.678	2.308
2 456 191.699846	−64.856	1.104
2 456 545.689792	−64.892	1.340

Table A.5. HE 0442−1234.

HJD	RV (km s^{-1})	$RV_{\rm err}$ (km s^{-1})
2 454 338.746568	231.895	0.043
2 454 373.755033	231.272	0.022
2 454 396.675349	231.387	0.045
2 454 406.673221	231.488	0.047
2 454 480.469787	231.625	0.037
2 454 496.400729	231.149	0.135
2 454 516.413321	231.777	0.020
2 454 705.704003	230.516	0.030
2 454 780.549248	230.670	0.046
2 454 793.526401	230.398	0.173
2 454 819.485376	231.059	0.041
2 454 852.550506	231.299	0.045
2 455 059.709842	254.627	0.039
2 455 079.721105	255.868	0.030
2 455 126.674591	252.221	0.032
2 455 149.614597	250.514	0.037
2 455 171.540400	248.975	0.021
2 455 207.416924	246.988	0.029
2 455 232.382885	245.710	0.030
2 455 439.745696	240.146	0.032
2 455 478.744628	239.853	0.067
2 455 531.646433	239.862	0.033
2 455 821.705466	236.600	0.024
2 455 944.486938	236.352	0.046
2 455 971.360048	236.071	0.040
2 456 191.737737	234.847	0.023
2 456 574.706961	233.444	0.020
2 456 956.723997	231.920	0.055

Table A.6. HE 0524−2055.

HJD	RV (km s^{-1})	$RV_{\rm err}$ (km s^{-1})
2 454 396.640800	255.070	0.185
2 454 406.717056	255.306	0.110
2 454 480.496860	255.712	0.098
2 454 820.481773	255.614	0.142
2 455 149.688274	255.624	0.084
2 455 207.491478	255.546	0.104
2 455 503.608363	255.614	0.551
2 455 531.544536	255.478	0.171
2 455 882.598085	255.358	0.108
2 456 005.376504	255.236	0.360
2 456 207.754219	255.340	0.082
2 456 603.661353	255.443	0.088
2 456 956.750015	255.185	0.196

Table A.7. HE 1044−2509.

HJD	RV (km s^{-1})	$RV_{\rm err}$ (km s^{-1})
2 454 909.489857	342.628	3.089
2 454 930.426948	369.639	1.671
2 455 174.767340	379.567	2.399
2 455 207.625989	362.229	1.939
2 455 620.563564	384.868	1.939
2 455 704.385256	343.075	2.077
2 455 712.405032	335.836	1.872
2 455 718.397062	358.699	2.243
2 455 722.397011	375.517	1.896
2 455 725.396840	386.965	3.807
2 455 730.395197	385.629	2.338
2 455 733.391004	378.210	3.132
2 455 738.401973	354.412	1.072
2 456 796.438819	363.768	1.346

Table A.8. HE 1105+0027.

HJD	RV (km s^{-1})	$RV_{\rm err}$ (km s^{-1})
2 454 459.682587	76.353	1.799
2 454 464.668667	76.746	1.762
2 454 516.585694	75.947	1.514
2 454 909.650314	75.405	0.794
2 455 232.610390	76.608	0.991
2 455 344.429621	76.620	1.860
2 455 531.735132	76.372	1.831
2 455 662.477811	76.280	1.239
2 456 033.449115	75.442	1.403

Table A.9. HE 1127−1143.

HJD	RV (km s^{-1})	$RV_{\rm err}$ (km s^{-1})
2 454 459.748479	229.676	2.402
2 454 481.662602	229.183	1.172
2 454 964.473253	228.850	1.277
2 455 232.656932	228.583	1.005
2 455 620.602643	229.334	1.314
2 455 662.541359	228.736	1.308
2 456 458.454152	229.734	0.725

Table A.10. HE 1219−0319.

HJD	RV (km s^{-1})	$RV_{\rm err}$ (km s^{-1})
2 454 481.728699	163.210	3.750
2 454 625.460187	162.919	1.680
2 455 620.657226	163.474	2.343
2 456 090.413526	161.166	2.464
2 456 652.702430	161.310	2.342

Table A.11. HE 1430+0053.

HJD	RV (km s^{-1})	$RV_{\rm err}$ (km s^{-1})
2 454 219.667720	−107.225	0.276
2 454 314.443374	−108.199	0.203
2 454 459.780220	−107.456	0.161
2 454 464.791534	−107.738	0.217
2 454 480.776288	−107.848	0.177
2 454 625.420967	−107.371	0.217
2 454 930.698058	−107.699	0.173
2 454 951.700884	−107.748	0.256
2 454 987.473997	−107.662	0.181
2 455 232.782505	−107.709	0.145
2 455 344.579755	−107.138	0.179
2 455 620.687317	−107.719	0.243
2 455 662.702207	−107.560	0.173
2 455 704.614991	−107.359	0.157
2 455 738.545590	−108.383	0.218
2 455 776.455326	−108.773	0.204
2 456 005.755704	−108.120	0.622
2 456 033.623529	−108.201	0.206
2 456 078.504562	−107.171	0.187
2 456 712.726996	−107.900	0.651

Table A.12. HE 1523−0901.

HJD	RV (km s^{-1})	$RV_{\rm err}$ (km s^{-1})
2 454 219.705449	−163.546	0.016
2 454 254.642226	−163.593	0.039
2 454 285.507316	−163.348	0.015
2 454 314.462351	−163.385	0.012
2 454 625.508366	−163.091	0.010
2 454 930.677427	−163.244	0.016
2 454 951.718880	−162.971	0.017
2 454 964.675531	−162.951	0.022
2 454 987.509060	−163.041	0.014
2 455 344.542474	−162.849	0.013
2 455 415.386096	−163.549	0.010
2 455 439.363821	−163.724	0.016
2 455 620.738975	−162.875	0.017
2 455 662.681656	−163.110	0.012
2 455 704.633870	−163.372	0.016
2 455 738.564258	−163.723	0.020
2 455 776.438140	−163.732	0.016
2 456 005.728789	−163.530	0.020
2 456 078.539561	−163.442	0.015
2 456 307.786409	−163.457	0.016
2 456 351.717323	−163.347	0.014
2 456 372.687769	−163.477	0.014
2 456 399.619896	−163.371	0.015
2 456 426.543882	−163.298	0.021
2 456 474.451216	−163.108	0.011
2 456 488.426825	−162.960	0.024
2 456 489.500440	−163.000	0.015
2 456 520.424407	−162.818	0.020
2 456 529.377789	−162.938	0.017
2 456 664.770980	−163.461	0.012
2 456 685.790500	−163.626	0.011
2 456 712.759468	−163.414	0.020
2 456 796.646910	−162.880	0.011
2 456 813.610868	−162.988	0.015

Table A.13. CS 22892−052.

HJD	RV (km s^{-1})	$RV_{\rm err}$ (km s^{-1})
2 454 314.576915	13.178	0.053
2 454 338.541838	13.553	0.136
2 454 373.414188	13.559	0.053
2 454 390.364640	13.579	0.079
2 454 625.684458	13.594	0.058
2 454 665.611641	13.917	0.063
2 454 705.568239	13.747	0.051
2 455 009.693164	13.480	0.098
2 455 059.511399	13.695	0.076
2 455 174.314885	13.374	0.050
2 455 415.522393	13.471	0.061
2 455 531.326532	13.467	0.108
2 455 704.706380	13.742	0.090
2 455 776.612557	13.367	0.049
2 455 822.600538	13.505	0.103
2 455 882.349889	13.624	0.051
2 456 139.644767	13.413	0.087
2 456 191.399426	13.585	0.099
2 456 488.673600	13.584	0.066

Table A.14. HE 2224+0143.

HJD	RV (km s^{-1})	$RV_{\rm err}$ (km s^{-1})
2 454 314.626987	−113.002	0.070
2 454 338.455766	−113.041	0.061
2 454 373.470335	−113.043	0.113
2 454 625.646394	−112.867	0.147
2 454 665.630399	−112.981	0.118
2 454 705.522460	−113.104	0.115
2 455 009.711530	−113.138	0.099
2 455 059.529868	−113.020	0.056
2 455 070.548978	−112.989	0.159
2 455 175.444551	−113.221	0.079
2 455 344.685686	−112.945	0.119
2 455 415.497735	−112.930	0.102
2 455 439.426753	−112.968	0.103
2 455 503.356818	−113.402	0.352
2 455 531.410900	−113.220	0.136
2 455 704.677515	−113.216	0.095
2 455 776.507942	−112.924	0.093
2 455 796.580352	−112.817	0.094
2 455 882.328613	−113.245	0.106
2 456 078.720195	−113.064	0.081
2 456 140.610920	−113.674	0.186
2 456 191.379978	−113.152	0.059
2 456 488.693610	−113.205	0.084
2 456 956.553882	−112.876	0.303

Table A.15. HE 2244−1503.

HJD	RV (km s^{-1})	$RV_{\rm err}$ (km s^{-1})
2 454 338.580931	147.980	1.346
2 454 373.501898	148.051	1.007
2 454 390.393739	148.275	1.573
2 454 665.675576	147.791	1.192
2 455 059.563356	147.724	1.446
2 455 149.413670	148.224	1.470
2 455 415.573319	148.194	1.123
2 455 439.540189	147.532	1.306
2 455 478.531528	147.567	0.899
2 455 738.686456	147.855	0.872
2 455 776.556273	147.947	1.562
2 455 822.637317	148.094	1.569
2 456 191.476165	148.111	0.922
2 456 545.578750	147.649	1.362

Table A.16. HD 221170.

HJD	RV (km s^{-1})	$RV_{\rm err}$ (km s^{-1})
2 454 314.636048	−121.161	0.010
2 454 338.524441	−121.179	0.009
2 454 373.528280	−121.107	0.009
2 454 390.345759	−121.253	0.010
2 454 406.586097	−121.114	0.011
2 454 480.397616	−121.164	0.013
2 454 625.656022	−121.267	0.012
2 454 705.500584	−121.138	0.017
2 454 780.452621	−121.111	0.012
2 454 793.471559	−121.182	0.011
2 454 820.348668	−121.321	0.014
2 455 009.719853	−121.078	0.011
2 455 059.695625	−121.185	0.009
2 455 071.639351	−121.199	0.017
2 455 171.399245	−121.340	0.008
2 455 344.693948	−121.230	0.011
2 455 415.506520	−121.259	0.012
2 455 439.446714	−121.227	0.008
2 455 503.346059	−121.358	0.014
2 455 531.470241	−121.412	0.011
2 455 704.717098	−121.256	0.009
2 455 738.710786	−121.253	0.018
2 455 776.728437	−121.333	0.012
2 455 796.566301	−121.342	0.011
2 455 859.532089	−121.249	0.009
2 455 892.424873	−121.011	0.029
2 455 915.320942	−121.166	0.077
2 456 140.740348	−121.075	0.010
2 456 241.340390	−121.056	0.013
2 456 488.721460	−121.000	0.010

Table A.17. CS 30315−029.

HJD	RV (km s^{-1})	$RV_{\rm err}$ (km s^{-1})
2 454 314.742671	−168.937	0.074
2 454 373.581743	−169.408	0.066
2 454 705.601838	−169.668	0.074
2 455 059.649134	−169.963	0.071
2 455 175.377253	−168.867	0.130
2 455 415.665073	−169.830	0.078
2 455 776.636347	−169.582	0.071
2 455 796.640879	−169.184	0.055
2 455 821.555408	−169.165	0.065
2 455 859.497621	−169.214	0.092
2 455 882.472080	−169.087	0.100
2 456 139.682491	−169.008	0.242
2 456 530.669987	−169.196	0.120
2 456 987.357305	−169.738	0.077

Appendix B: Literature data for the programme stars

Table B.1. Mean heliocentric radial velocities from the literature and total time-span covered for the single stars.

Star ID	ΔT Total (days)	$\bar{RV}$ (this work) (km s^{-1})	$\bar{RV}$ (lit) (km s^{-1})	N	Ref.
HD 20	10011	−57.914	−57.4	3	Carney & Latham (1986)
			−57.2	13	Carney et al. (2003)
			−57.5	1	Barklem et al. (2005)
CS 29497−004	4742	+105.008	+105.1	1	Barklem et al. (2005)
CS 31082−001	5193	+139.068	+139.1	8	Hill et al. (2002)
			+138.9	2	Aoki et al. (2003)
			+138.2	1	Tsangarides et al. (2003)
			+138.9	1	Honda et al. (2004)
			+139.4	1	Barklem et al. (2005)
			+139.0	1	Carrera et al. (2013)
			+138.4	1	Kordopatis et a. (2013)
			+138.9	1	Roederer et al. (2014a)
HE 0432−0923	3582	−64.800	−66.6	1	Barklem et al. (2005)
HE 0524−2055	4032	+255.425	+255.3	1	Barklem et al. (2005)
HE 1105+0027	3267	+76.197	+77.0	1	Barklem et al. (2005)
HE 1127−1143	3785	+229.157	+228.5	1	Barklem et al. (2005)
HE 1219−0312	3885	+162.416	+163.6	1	Barklem et al. (2005)
			+163.1	5	Hayek et al. (2009)
HE 1430+0053	3942	−107.749	−107.4	1	Barklem et al. (2005)
CS 22892−052	8788	+13.549	+13.1	10	McWilliam et al. (1995)
			+13.6	1	Norris et al. (1996)
			+12.5	15	Preston & Sneden (2001)
			+13.2	1	Aoki et al. (2003)
			+12.7	1	Honda et al. (2004)
			+14.5	1	Barklem et al. (2005)
			+13.3	1	Bonifacio et al. (2009)
			+13.0	2	Roederer et al. (2014a)
HE 2224+0143	3968	−113.085	−112.3	1	Barklem et al. (2005)
HE 2244−1503	3960	+147.928	+148.1	1	Barklem et al. (2005)
HD 221170	10921	−121.201	−119.0	4	Wilson (1953)
			−123.7	3	Wallerstein et al. (1963)
			−121.8	18	Carney et al. (2003)
			−120.7	1	Barklem et al. (2005)
			−121.7	1	Carney et al. (2008)
			−121.8	1	Soubiran et al. (2008)
CS 30315−029	4741	−169.346	−169.2	1	Barklem et al. (2005)

Table B.2. Mean heliocentric radial velocities for single stars not included in the programme.

Star ID	ΔT Total (days)	$\bar{RV}$ (km s^{-1})	N	Ref.
HD 115444	8812	−27.6	3	Griffin et al. (1982)
		−26.2	2	Bartkevicius et al. (1992)
		−27.1	2	Aoki et al. (2003)
		−27.2	1	Famaey et al. (2005)
HD 122563	21575	−26.1	3	Wilson (1950)
		−26.5	6	Wallerstein et al. (1963)
		−24.9	6	Woolley (1965)
		−26.0	1	Bond (1980)
		−26.0	1	Roederer et al. (2008)
		−26.4	1	Bonifacio et al. (2009)
		−25.6	2	Hollek et al. (2011)
		−26.1	3	Roederer et al. (2014a)